**LETTER • OPEN ACCESS**

# Warm Arctic−cold Siberia: comparing the recent and the early 20th-century Arctic warmings

View the article online for updates and enhancements.

# Environmental Research Letters

**LETTER**

# Warm Arctic—cold Siberia: comparing the recent and the early 20th-century Arctic warmings

**Martin Wegmann**[1,2,3,6] , **Yvan Orsolini**[4] **and Olga Zolina**[1,5]

1   Institut des Géosciences de l'Environnement, University of Grenoble, Grenoble, France
2   Oeschger Centre for Climate Change Research, University of Bern, Bern, Switzerland
3   Institute of Geography, University of Bern, Bern, Switzerland
4   NILU—Norwegian Institute for Air Research, Kjeller, Norway
5   Shirshov Institute of Oceanology, RAS, Moscow, Russia
6   Author to whom any correspondence should be addressed.

**E-mail:** martin.wegmann@univ-grenoble-alpes.fr

## Abstract

The Warm Arctic–cold Siberia surface temperature pattern during recent boreal winter is suggested to be triggered by the ongoing decrease of Arctic autumn sea ice concentration and has been observed together with an increase in mid-latitude extreme events and a meridionalization of tropospheric circulation. However, the exact mechanism behind this dipole temperature pattern is still under debate, since model experiments with reduced sea ice show conflicting results. We use the early twentieth-century Arctic warming (ETCAW) as a case study to investigate the link between September sea ice in the Barents–Kara Sea (BKS) and the Siberian temperature evolution. Analyzing a variety of long-term climate reanalyses, we find that the overall winter temperature and heat flux trend occurs with the reduction of September BKS sea ice. Tropospheric conditions show a strengthened atmospheric blocking over the BKS, strengthening the advection of cold air from the Arctic to central Siberia on its eastern flank, together with a reduction of warm air advection by the westerlies. This setup is valid for both the ETCAW and the current Arctic warming period.

## 1. Introduction

Arctic sea ice extent has declined steadily by more than 10% per decade since the start of the satellite era (e.g. Stroeve *et al* 2011). While negative tendencies are observed for all seasons throughout the year, the most pronounced decline is observed in late summer and early autumn (Serreze *et al* 2007). Together with this sea ice decline, a strong near-surface Arctic warming has been recorded, especially during boreal wintertime (Screen and Simmonds 2010), attributed to the Arctic amplification of anthropogenic global warming (Serreze and Barry 2011). This amplification is characterized by Arctic temperature trends which are approximately twice as strong as the hemispheric trends (Semenov *et al* 2010).

This well-documented Arctic warming trend has been observed in conjunction with a winter cooling of the mid-latitudes in recent years, being particularly strong over central Siberia (Cohen *et al* 2014, Vihma 2014, Shepherd 2016, Overland *et al* 2016 and references therein). Patterns of intensified cold spells and extreme snowfall events were also documented over the other Northern Hemisphere mid-latitude regions (Cohen *et al* 2007, Ghatak *et al* 2012, Vihma 2014, Wegmann *et al* 2015, Orsolini *et al* 2016). The Eurasian variant of this phenomenon has been termed 'warm Arctic–cold Siberia,' or WACS—similar definitions such as 'warm Arctic–cold Eurasia' are essentially describing the same pattern (Petoukhov *et al* 2013)—since the appearance of a cold anomaly over Siberia was found in conjunction with warming over the Barents–Kara Sea (BKS) region (Overland *et al* 2011, Inoue *et al* 2012).

Several studies investigated the possible mechanisms behind this counterintuitive process. Honda *et al* (2009) first demonstrated that the WACS pattern can be attributed to sea ice loss over the BKS, which in

turn triggers increased turbulent heat fluxes from the ocean to the atmosphere. It was found that an increasing autumn surface heat flux from the open waters to the cooler atmosphere with anomalous warming of the lower atmosphere triggers increased baroclinic wave activity and higher amplitudes of Rossby waves, which favor the development of blockings and extreme weather such as cold air outbreaks (Francis *et al* 2009, Honda *et al* 2009, Orsolini *et al* 2012, Cohen *et al* 2014, Mori *et al* 2014, Jaiser *et al* 2016, Nakamura *et al* 2016, Luo *et al* 2016, Sorokina *et al* 2016). Understanding the causes of such extreme events is therefore of large societal importance (Overland *et al* 2016, Francis 2017).

There remains uncertainty about whether the winter WACS pattern is a delayed response to decreased autumn sea ice (Honda *et al* 2009, Overland *et al* 2011, Wegmann *et al* 2015, Suo *et al* 2016, Wu 2017) via a stratospheric feedback (Jaiser *et al* 2012, Cohen *et al* 2014, García-Serrano *et al* 2015, Jaiser *et al* 2016, Ruggieri *et al* 2017, Kretschmer *et al* 2017) or if it is an immediate response triggered by winter sea ice anomalies (Hori *et al* 2011, Inoue *et al* 2012, Sorokina *et al* 2016, King *et al* 2016). The physical feedbacks, as summarized by Cohen *et al* (2014), are thought to induce a causal chain process, where reduced autumn sea ice warms the lower troposphere, which increases geopotential heights, shifts stormtracks and increases Eurasian snow cover in October and November. This setting favors high Rossby wave numbers, with vertical propagation of Rossby wave energy, resulting in a weakening polar vortex and a stratospheric warming event (Gastineau *et al* 2017). Subsequently, tropospheric circulation anomalies appear with a few weeks' lag.

Despite the uncertainty of the temporal relationship, the BKS region emerges as the core region for atmospheric feedbacks triggering the WACS (Inoue *et al* 2012, Outten *et al* 2013, Luo *et al* 2016, Zhang *et al* 2016, Screen 2017). Reduction in BKS sea ice can be caused by several mechanisms, including warm Atlantic water inflow (Miles *et al* 2014, Nakanowatari *et al* 2014, Årthun *et al* 2017), atmospheric heat advection (Zhang and Li 2017) or atmospheric radiation feedbacks (Park *et al* 2015).

Recent studies based on sensitivity experiments with atmospheric global climate models (AGCMs) nevertheless question the proposed link between sea ice reduction and the WACS pattern (Sato *et al* 2014, Sun *et al* 2016, McCusker *et al* 2016, Boland *et al* 2017, Collow *et al* 2016). On the other hand, some model studies (Honda *et al* 2009, Nakamura *et al* 2015, Kretschmer *et al* 2017, Pedersen *et al* 2016, Crasemann *et al* 2017, Ruggieri *et al* 2017) did indeed show realistic tropospheric sensitivity to sea ice forcing. Cohen *et al* 2012 as well as Cohen 2016 pointed out that many of the current generation of AGCMs may lack the ability to simulate the influence of Arctic amplification on mid-latitude climate. This raises the question of whether the WACS pattern can result from the random sampling of climate states undergoing chaotic nonlinear variability, or rather is being controlled by the proposed causal link to sea ice, but with this physical mechanism missed in the state-of-the-art AGCMs (Francis 2017).

Here we utilize long-term reanalyses and reconstruction datasets to investigate the 'early twentieth-century Arctic warming' (ETCAW) which reached its peak warming at the beginning of the 1940s but started around 1910. Compared to the present Arctic warming, the ETCAW was mainly confined to the European Atlantic sector (Scherhag 1939, Bengtsson *et al* 2004, Wood and Overland 2010, Bekryaev *et al* 2010). In the vertical, recent maximums of temperature anomalies are mostly found at the surface whereas the maximum warming of the ETCAW was located in the mid troposphere (Grant *et al* 2009, Brönnimann *et al* 2012). Possible warming mechanisms include warm air advection by southerly winds (Wood and Overland 2010, Wegmann *et al* 2017) as well as increased winter sea-surface temperatures (SSTs) (Johannessen *et al* 2004, Bengtsson *et al* 2004, Semenov and Latif 2012). Analyzing 26 simulated Arctic warming events, Beitsch *et al* (2014) found a triggering warming ocean signal that induces atmospheric changes, including increased stationary eddy heat transport into the Arctic domain. Recently, Tokinaga *et al* (2017) were able to reproduce the large-scale ETCAW by introducing historical SST forcing in an atmosphere–ocean coupled global climate models (AOGCM), underlining the importance of SSTs in the onset and evolution of the ETCAW.

Paleoclimatic data suggest that, until the beginning of the twenty-first century, the ETCAW was unique in magnitude and rate for at least the last 1500 years in the Arctic domain (Kaufman *et al* 2009, Pages 2 K Consortium 2013, Opel *et al* 2013). Therefore, the ETCAW offers a unique opportunity to investigate feedbacks of global climate during Arctic warming periods.

The goal of this study is to demonstrate the consistency between both periods, of the sea ice decline, the covariability of the sea ice with atmospheric temperature and heat fluxes, and their impact on the Arctic region. For this purpose, we compare decadal temperature trend patterns among the two warming events (ETCAW and present) and the dynamical conditions leading to the associated WACS pattern. We focus on the boreal winter (DJF) temperatures and their relationship with September sea ice extent in the BKS region using regression analysis for quantifying the role of different mechanisms.

The paper is organized as follows: section 2 describes the data and methods used. In section 3 we introduce the ETCAW and the respective WACS patterns, whereas section 4 investigates the dynamical process behind that pattern. These results are discussed in section 5 and finally summarized in section 6.

## 2. Data and methods

### 2.1. Atmospheric reanalyses

To investigate the dynamical processes behind the WACS pattern we use a variety of atmospheric reanalysis products. To analyze the current warming we use ERA-Interim reanalysis (Dee *et al* 2011) which was widely used in different applications including Arctic processes (eg. Lindsay *et al* 2014, Dufour *et al* 2016).

To investigate the ETCAW we mainly use the European Centre for Medium-Range Weather Forecasts (ECMWF) ERA-20C (ERA20C) reanalysis (Poli *et al* 2016). ERA-20C uses the Integrated Forecast System (IFS) as a framework to assimilate observations of surface pressure and surface marine winds. It has global coverage for the period 1900–2010 with a 3 hourly temporal resolution and a horizontal resolution of 1 degree with 91 vertical levels from the surface up to 1 Pa. Sea ice cover and SST forcing come from the HadISST.2.1 reconstruction (Titchner and Rayner 2014). Comparisons to other long-term reanalyses can be found in the supplement.

### 2.2. Reconstruction data

For near-surface air temperature reconstruction we use the National Aeronautics and Space Administration (NASA) Goddard Institute for Space Studies (GISS) Surface Temperature Analysis (GISTEMP) dataset (Hansen *et al* 2010, https://data.giss.nasa.gov/GISTEMP/). This dataset offers a homogeneous reconstruction of global temperature based on historical station data back to 1880 with a $2° \times 2°$ resolution. We use both the Land-Ocean Temperature Index which uses reconstructed SSTs (ERSSTv4) to fill in data gaps over the oceans (smoothing radius 1200 km) as well as the station-only dataset (smoothing radius 20 km).

### 2.3. Global climate model

To assess the relative impact of internal and external variability, we compare reanalysis datasets with an ensemble model experiment. The ECMWF integrated an ensemble of ten Integrated Forecast System (IFS) atmospheric simulations for the years 1899–2009 at a horizontal resolution of 1 degree with 91 vertical levels reaching from the surface up to 1 Pa, known as the final ERA-20 cm version (ERA20CM). Specified sea ice concentration as well as sea-surface temperature boundary conditions come from HadISST.2 (same as ERA20C) and the radiation scheme follows the CMIP5 protocol exactly, including aerosols, ozone and greenhouse gases (Hersbach *et al* 2015). Both in the GCM and the reanalyses we use integrated heat-flux values, which are integrated over all model levels in the IFS model of the respective ECMWF dataset.

### 2.4. Sea ice data

For recent sea ice data we use the ERA-Interim sea ice concentration (SIC), which is highly correlated to the NSIDC sea ice data. For instance, Sorokina *et al* (2016) reported no differences between these two datasets.

For the ETCAW period we investigate five different SIC datasets, namely the three products used in the long-term reanalyses (see table 1) as well as the independent sea ice concentration data by Walsh *et al* (2017) plus the sea ice output from the centennial ocean reanalysis ORA-20C by the ECMWF (De Boisséson *et al* 2017). Although there are considerable uncertainties regarding the Arctic sea ice conditions before 1950, Connolly *et al* (2017) recently provided a new reconstruction of historical Arctic sea ice which supported the melting period between 1910–1940. Moreover, Alekseev *et al* (2016) found a substantial decrease of September Arctic sea ice between 1930–1940 in their assessment of Arctic sea ice in the 20th century. Thus, besides the reconstructions used in this study, other independent datasets suggest a sea ice reduction during the ETCAW period.

We define the BKS as region bounded by 30–90° E, 65–85° N and focus on September sea ice. In September, sea ice reaches its annual minimum and open-water regions provide a strong heat and moisture release to the cold Arctic atmosphere (Jaiser *et al* 2016). We checked using different autumn months between September and December and found that regression with September sea ice best represents the DJF temperature trend, especially so for the ETCAW (see supplementary figure 1 available at stacks.iop.org/ERL/13/025009/mmedia). However, we did not find a large difference among all autumn months. All sea ice time series are normalized with respect to their time periods (1987–2016 for the current warming and 1911–1940 for the ETCAW). Luo *et al* (2016) found no notable difference between using original and de-trended sea ice time series in their feedback study (which we confirmed in supplementary figure 2), therefore we use original time series from here on. This highlights the fact that interannual variability is a key factor for investigating feedbacks rather than the overall trend. Figure 1 shows the normalized BKS sea ice concentration time series for all reconstructions, including both warming periods (for un-normalized BKS sea ice time series see supplementary figure 3). As can be seen, differences in reconstructions for the ETCAW can reach up to one standard deviation. However, when taken as average, the ETCAW BKS sea ice evolution is very similar to the recent BKS sea ice decrease. Therefore, it seems reasonable to use the ETCAW as an analogue (in terms of BKS sea ice impacts) to the recent Arctic warming (RAW) period.

### 2.5. Regression on SIC

We use the above-mentioned normalized BKS SIC time series to investigate linear relationships between atmospheric variables and the sea ice evolution. For
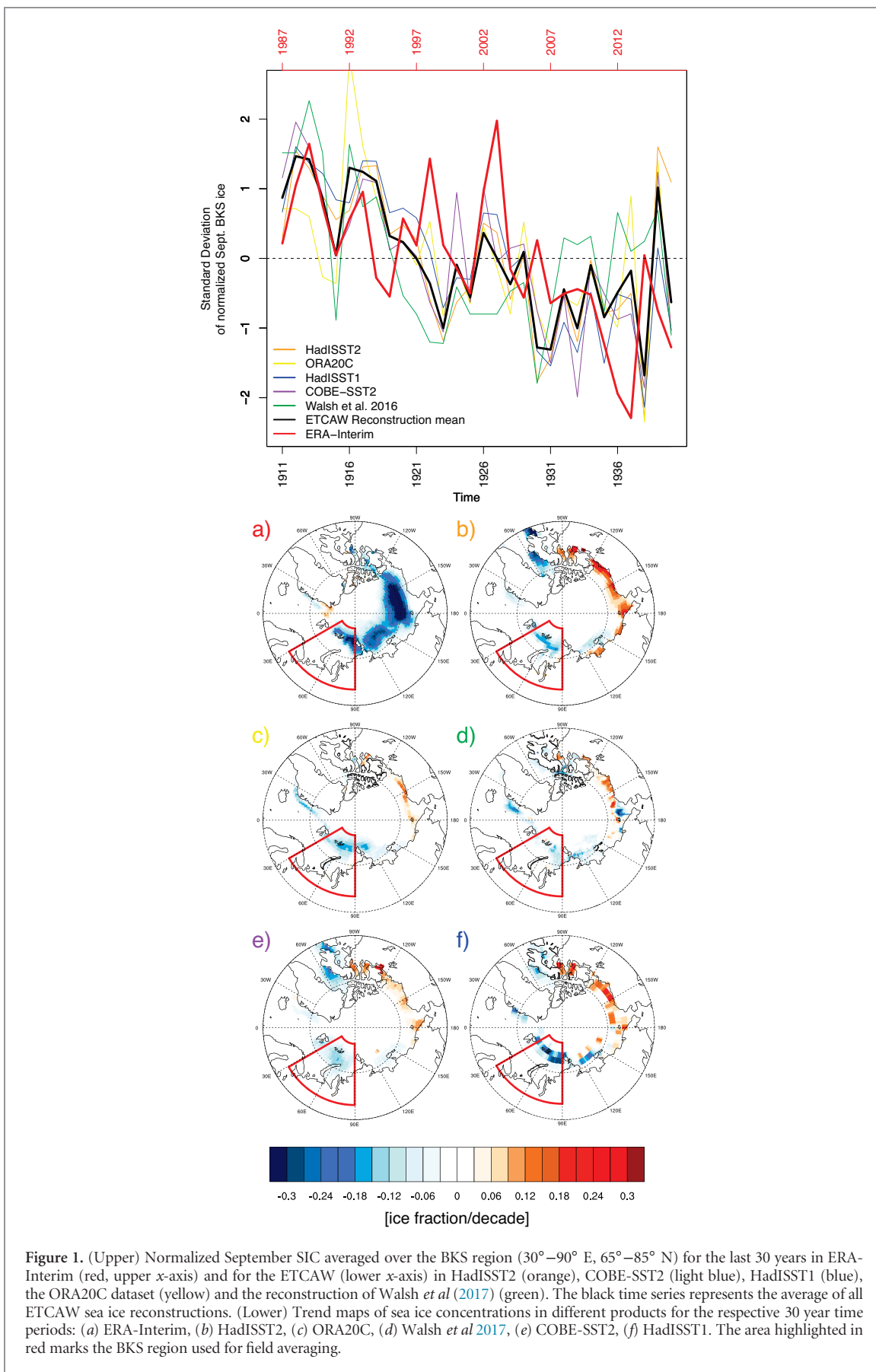
**Figure 1.** (Upper) Normalized September SIC averaged over the BKS region (30°−90° E, 65°−85° N) for the last 30 years in ERA-Interim (red, upper *x*-axis) and for the ETCAW (lower *x*-axis) in HadISST2 (orange), COBE-SST2 (light blue), HadISST1 (blue), the ORA20C dataset (yellow) and the reconstruction of Walsh *et al* (2017) (green). The black time series represents the average of all ETCAW sea ice reconstructions. (Lower) Trend maps of sea ice concentrations in different products for the respective 30 year time periods: (*a*) ERA-Interim, (*b*) HadISST2, (*c*) ORA20C, (*d*) Walsh *et al* 2017, (*e*) COBE-SST2, (*f*) HadISST1. The area highlighted in red marks the BKS region used for field averaging.

**Figure 2.** Trends [K/decade] of 2 m DJF temperatures (color shading) for the RAW (left column) in (*a*) ERA-Interim, (*b*) GISTEMP and the ETCAW (right column) in (*c*) ERA20C, (*d*) GISTEMP, (*e*) ERA20CM best guess member, (*f*) ERA20CM ensemble mean. Shading indicates 90% significance level.
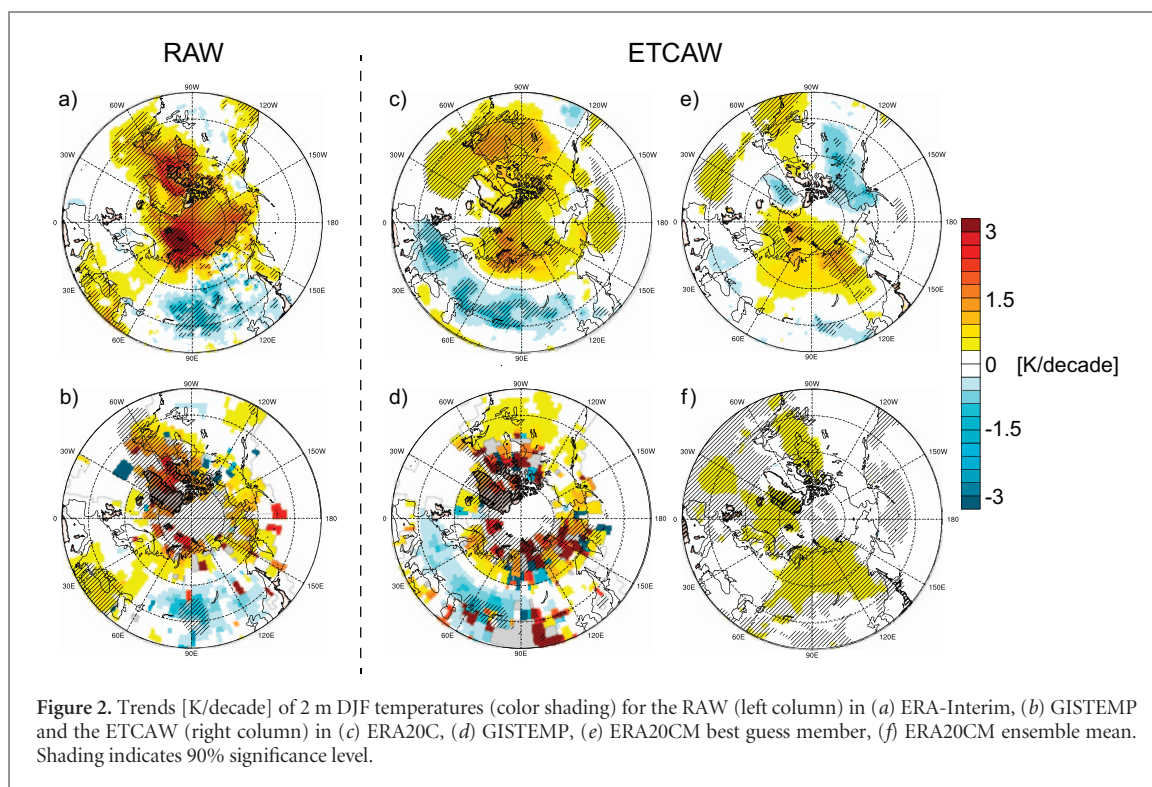
this purpose, we project the respective anomaly fields onto the SIC time series for the ETCAW period 1911–1940 and the RAW period 1987–2016. For the main manuscript it will be the normalized HadISST2 BKS SIC time series for the ETCAW and the normalized ERA-Interim BKS SIC time series for the RAW. To test the regression coefficient against the null hypothesis, we use a two-sided Student's *t*-test, which is also used for inferring the significance of the trends. For enhanced readability, the regressed fields are multiplied by −1 to correspond to a signal resulting from reduced sea ice.

## 3. Results

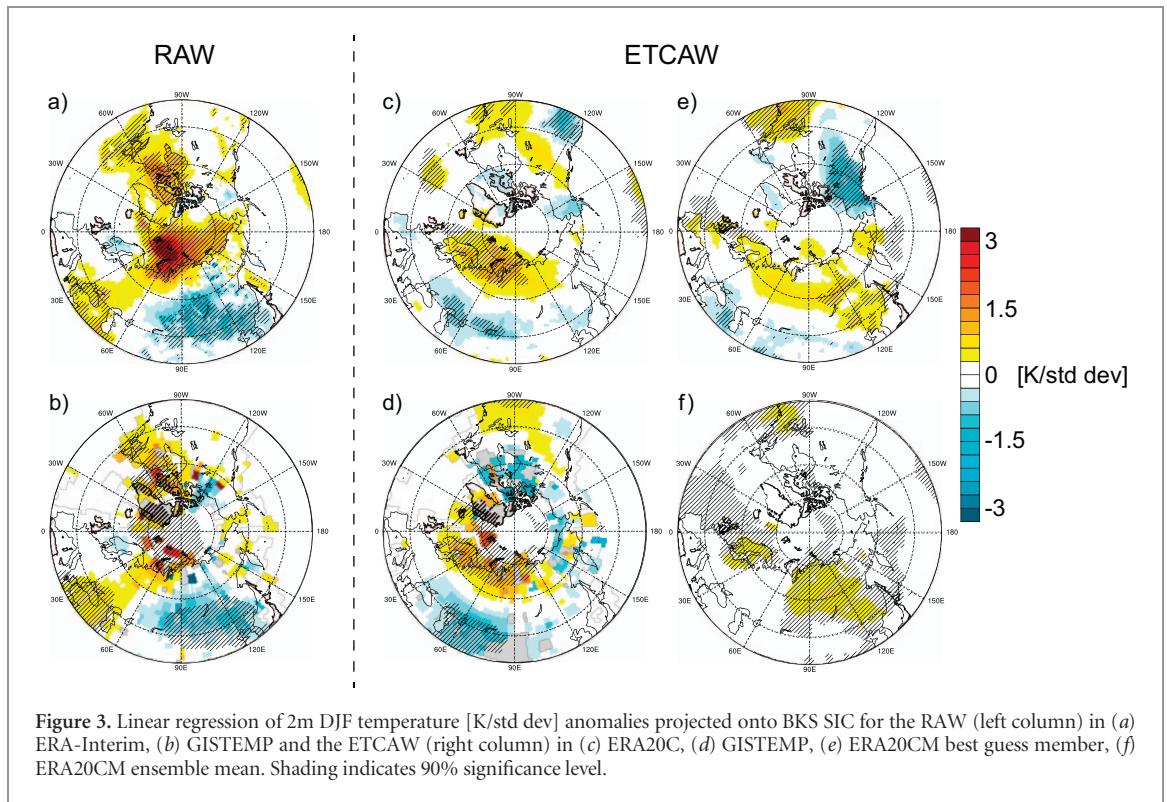### 3.1. Eurasian temperature patterns during Arctic warmings

Figure 2 shows that the WACS pattern can be identified for both warming periods (see supplementary figure 4 for the general Arctic winter temperature evolution). For the RAW, regions of negative trends are confined to central Siberia, and significant warming trends are found over the whole Arctic with the strongest signals identified over the BKS region. For the ETCAW, the cooling pattern is more widespread and extends to most of the European mid-latitudes. The warming trend over the Arctic is less intense than in the RAW, but the BKS region appears again as the key region for temperature increase. Alternatively, this WACS pattern displayed in the trends can be identified as the second empirical orthogonal function (EOF) pattern of 2m DJF temperatures over Eurasia (0°−180° E, 40°−90 °N), which exhibits a strong upswing

during the period 1911–1940, which is unique for the 20th century (see supplementary figure 5).

Interestingly, whilst widespread warming is visible for most of the mid-latitude and Arctic regions, yet the WACS signal is not visible in the ensemble mean of ERA20 CM, although the same boundary conditions were used for the ERA20C product.. As expected for an ensemble mean, trends are much weaker. We identified one member of the ensemble as 'best guess' (based on field correlation of the trend fields with regards to ERA20C), which expresses a somewhat similar NH temperature pattern but misses the homogeneous mid-latitude cooling.

The ERA20CM ensemble mean does not reproduce the observed temperature pattern, although ERA20CM is forced by the realistic SIC. Since the cooling is counterintuitive given anthropogenic global warming, local or dynamic processes must lead to the observed regional cooling pattern. Here, we investigate the impact of tropospheric heat transport associated with sea ice reduction.

To investigate one possible driver behind these trends, figure 3 shows the same structure as figure 2, but instead of trends over time, it shows linear regression of 2 m DJF temperature [K/std dev] anomalies projected onto the normalized BKS SIC time series (ERA-Interim September BKS sea ice 1987–2016 for the RAW, HadISST2 September BKS sea ice 1911–1940 for the ETCAW). In this analysis for the RAW period we used the ERA-Interim sea ice, whereas for the ETCAW period we used the HadISST2.0 dataset. Interestingly, spatial patterns in figure 3 look nearly identical to the trend patterns (figure 2), suggesting that September BKS SIC is an important driver of the

**Figure 3.** Linear regression of 2m DJF temperature [K/std dev] anomalies projected onto BKS SIC for the RAW (left column) in (*a*) ERA-Interim, (*b*) GISTEMP and the ETCAW (right column) in (*c*) ERA20C, (*d*) GISTEMP, (*e*) ERA20CM best guess member, (*f*) ERA20CM ensemble mean. Shading indicates 90% significance level.

temperature distribution, showing a clear temperature decrease between the Eurasian Arctic and the mid-latitudes. The strongest cold anomalies over Siberia are located further east in the RAW period compared to the ETCAW period, when the negative anomalies reach westwards into Central Europe. ERA20C shows slightly weaker anomalies than GISTEMP, where the best guess ensemble member of ERA20CM shows some resemblance to ERA20C, but the pattern does not hold statistical significance. The ERA20CM ensemble mean does not show any resemblance to the GISTEMP field.
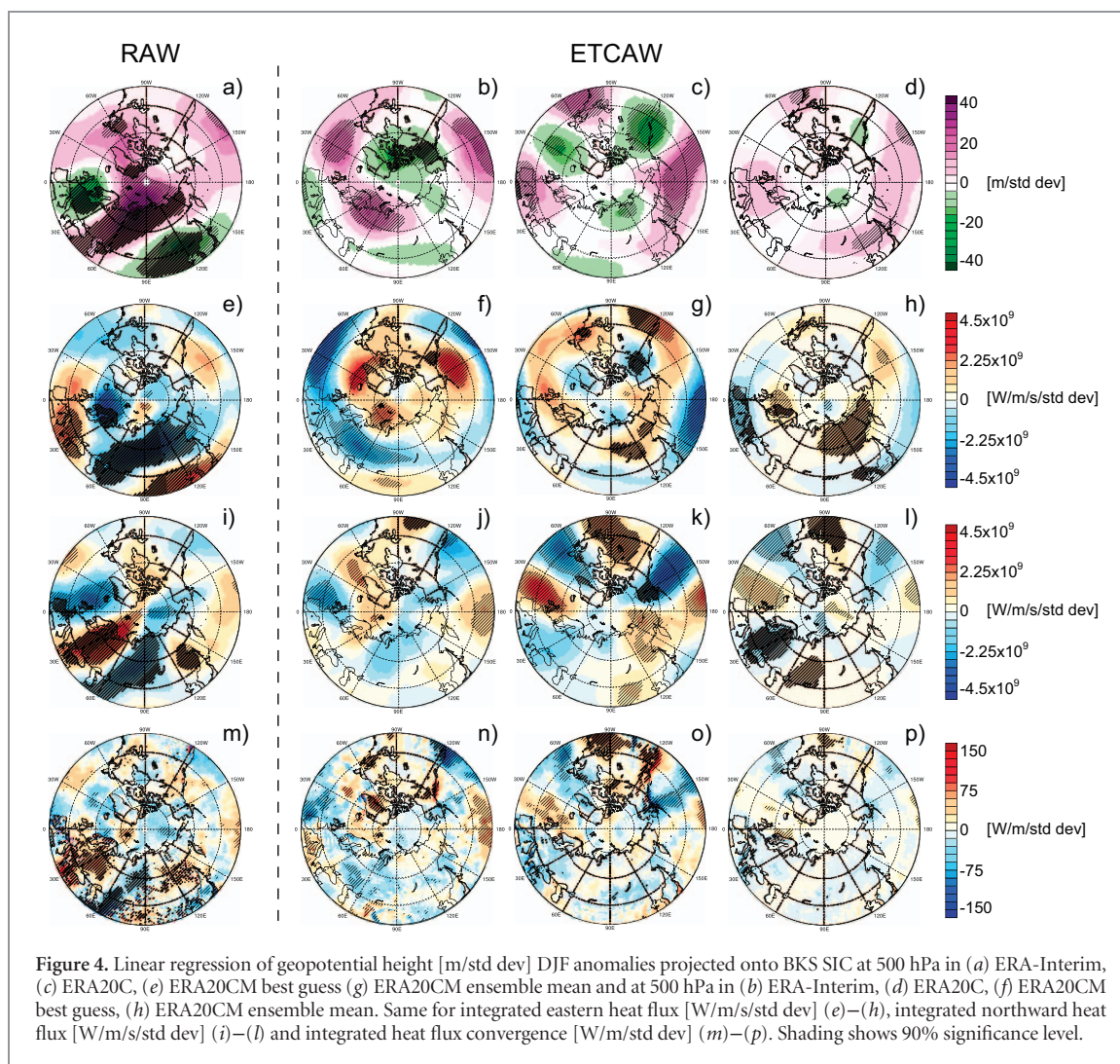
### 3.2. Tropospheric dynamics associated with sea ice loss

To investigate the tropospheric dynamics associated with the WACS pattern, figures 5(*a*)−(*d*) shows 500 hPa geopotential anomalies regressed onto the same BKS SIC time series that were used in previous figures. For the RAW, a strong positive anomaly dominates the Arctic, extending southward over western Russia and reaching the Caspian Sea. This high-pressure anomaly is flanked by two low-pressure systems leading to a zonal-to-meridional transition of the heat advection. For the ETCAW in ERA20C, a similar structure can be observed for Eurasia. Using the Walsh *et al* (2017) or ORA20C dataset, this transition becomes even more apparent (see supplementary figure 6).

The geopotential height patterns shown figures 4(*a*)−(*d*) cause anomalous heat advection over the Eurasian domain. We regressed horizontal heat-flux anomalies onto the BKS SIC time series to investigate the response of atmospheric heat transport to the SIC signals during ETCAW and RAW (figures 4(*e*)−(*p*)).

For the RAW, a wave train-like structure in meridional heat flux (figures 4(*i*)-(*l*)) over Europe and Eurasia is clearly visible as well as the westward heat flux over northern Europe and Siberia. This means that cold air is transported southward from the Arctic into large parts of eastern Siberia. Moreover, the westward pattern over the mid-latitudes combined with the strong waviness reduces heat advection by westerlies, which usually advect warm, maritime air masses. For the ETCAW, ERA20C shows eastward heat flux over large parts of the Central Arctic with Atlantic air masses being advected to Northern Russia. Meridional heat-flux patterns in ERA20C are homologous to the trend pattern as well, with southward fluxes from the Arctic towards Central Siberia. We note, that the wave train-like pattern in meridional heat flux derived by regressing heat fluxes onto HadISST2.0 SIC over Eurasia does not hold statistical significance. However, using the Walsh *et al* (2017) or the ORA20C sea ice reconstruction together with ERA20C atmospheric fields, the southward cold-air transport becomes significant and the transport pattern largely resembles the RAW pattern (see supplementary figure 7). As for the RAW, the westward circulation over large parts of the Eurasian mid-latitudes reduces the advection of maritime air masses, supporting the cooling by the Arctic air masses coming from the north.

For the ERA20CM selected 'best guess' member, regression patterns are different from the ERA20C. The regression pattern shows no significant mid-latitude heat advection reduction but instead widespread eastward heat-flux increase in response to the SIC evolution, similar to the ERA20CM ensemble mean. This

**Figure 4.** Linear regression of geopotential height [m/std dev] DJF anomalies projected onto BKS SIC at 500 hPa in (*a*) ERA-Interim, (*c*) ERA20C, (*e*) ERA20CM best guess (*g*) ERA20CM ensemble mean and at 500 hPa in (*b*) ERA-Interim, (*d*) ERA20C, (*f*) ERA20CM best guess, (*h*) ERA20CM ensemble mean. Same for integrated eastern heat flux [W/m/s/std dev] (*e*)−(*h*), integrated northward heat flux [W/m/s/std dev] (*i*)−(*l*) and integrated heat flux convergence [W/m/std dev] (*m*)−(*p*). Shading shows 90% significance level.
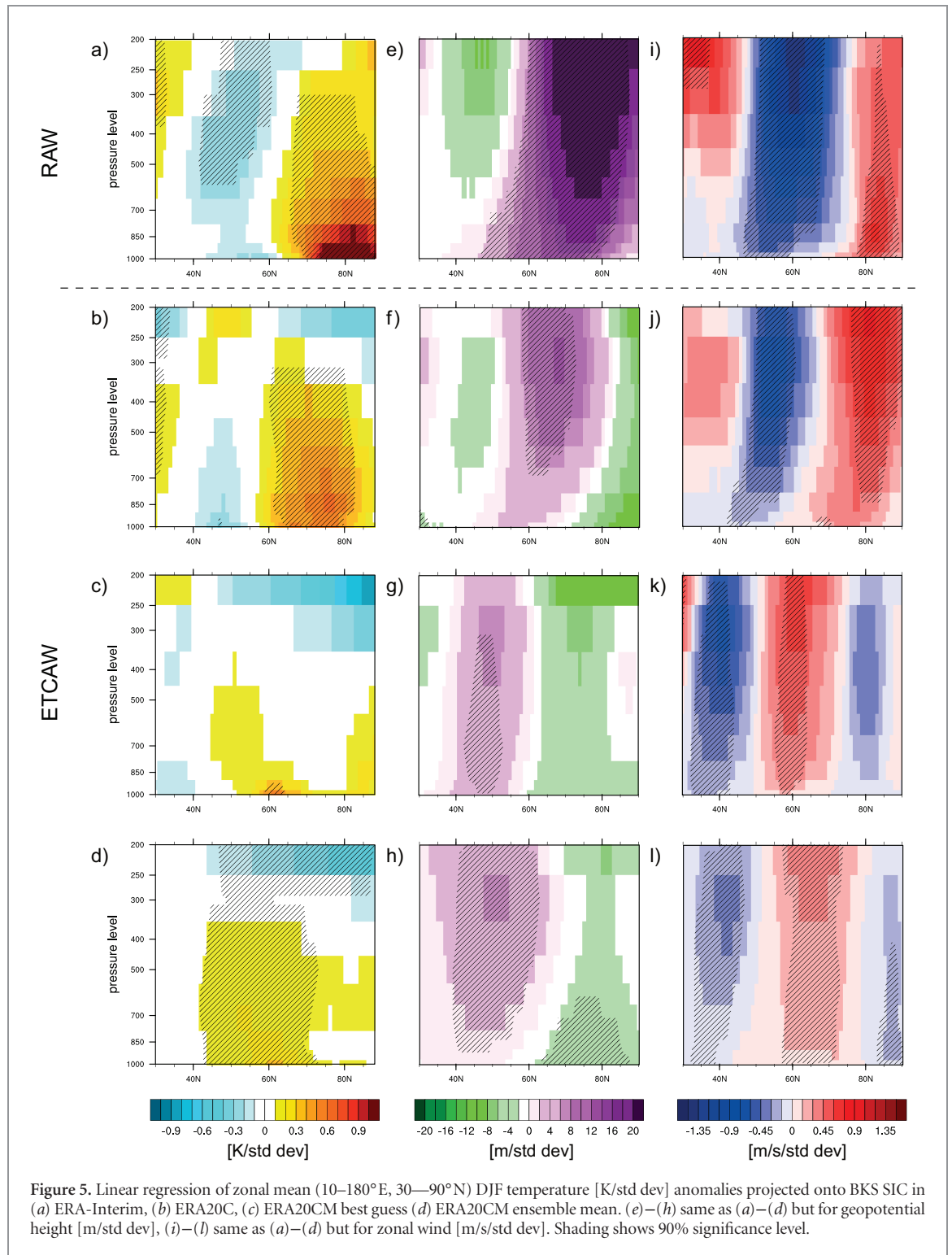
similarity is even more striking in the case of Arctic to mid-latitude heat transport, where the wave train-like structure over Eurasia shows the opposite sign to the heat transport in ERA20C.

Based on the comparison between the trend and regression patterns, we find that the overall winter temperature and heat-flux trend is largely congruent to a reduction of September BKS sea ice. Both eastward zonal flux and meridional flux culminate in integrated heat flux convergence (figures 4(*m*)−(*p*)), which shows a clear negative signal over Central Siberia for the ETCAW, and a little bit further to the east in the case of the RAW. Since ERA20CM already failed to reproduce the horizontal heat fluxes, no such areas of negative heat convergence can be found in the model fields.

In general, the structure of geopotential height anomalies in ERA20C is visible in neither the ERA20CM selected best guess member, nor the ensemble mean. Thus, the resulting heat-flux advection in ERA20CM is unlike what the reanalyses show. Moreover, this indicates that the influence of the sea ice on the models is not strong enough to reach the mid- and upper troposphere in the same way as is proposed in reanalyses.

Differences between reanalyses and the AGCM become even more striking when looking at the zonal mean temperature response to BKS SIC evolution throughout the troposphere over northern Eurasia (figure 5). Comparing the RAW (figure 5(*a*)) and ETCAW (figure 5(*b*)) temperature distribution reveals the strong gradient between the Arctic and the mid-latitude. The Arctic experiences a strong warming deep into the troposphere whereas south of 60°N the signal turns to a cooling that dominates the whole troposphere for the RAW and up to 300 hPa for the ETCAW. Note that the surface cooling is not significant for ERA-Interim, which is probably based on the chosen domain for the zonal average (10–180° E, 30–90° N) since eastern Europe shows a warming response for the RAW. Again, the mid-latitude cooling response in ERA20C can be strengthened by using different sea ice reconstructions. However, the structure of the WACS stays the same, regardless of the sea ice reconstruction or the reanalysis at hand (supplementary figure 8). Zonal mean plots of geopotential heights (figures 5(*e*)−(*f*)) show nicely the elevated geopotential height (GPH) values over and the Arctic in periods of Arctic warming. Differences between the RAW and ETCAW

**Figure 5.** Linear regression of zonal mean (10–180° E, 30—90° N) DJF temperature [K/std dev] anomalies projected onto BKS SIC in (*a*) ERA-Interim, (*b*) ERA20C, (*c*) ERA20CM best guess (*d*) ERA20CM ensemble mean. (*e*)−(*h*) same as (*a*)−(*d*) but for geopotential height [m/std dev], (*i*)−(*l*) same as (*a*)−(*d*) but for zonal wind [m/s/std dev]. Shading shows 90% significance level.

appear in the northern most gridboxes, where the ETCAW shows slightly reduced GPH values in the lower troposphere. As a consequence of the GPH nega-tive gradient between the Arctic and the mid-latitudes, a strongly reduced zonal wind appears throughout the troposphere in both Arctic warming cases, reach-ing from roughly 40°–60° N. These reduced zonal winds are connected to the reduced eastern heat flux shown in figures 4(*e*)−(*h*).

On the other hand, both the ERA20CM best guess member (figure 4(*c*)) and the ensemble mean

(figure 4(*d*)) show no mid-latitude cooling in response to the BKS SIC. Instead widespread tropospheric warming can be found in the mid-latitudes. The ERA20CM best guess member even fails to reproduce the widespread tropospheric warming response over the Arctic. Moreover, both ERA20CM analysis fields show nearly mirrored zonal mean zonal wind fields (figures 5(*k*)−(*l*)) compared to the reanalyses. Increased zonal wind dominates the mid-latitudes between 40°–60° N, which is a result of shifted geopo-tential height locations.

## 4. Discussion

We used a variety of gridded atmospheric datasets: AGCM simulations, reanalyses and reconstructions, to address some of the open questions regarding the cause and manifestation of the WACS surface temperature pattern—one of the most remarkable counterintuitive features associated with Arctic amplification.

A key question in the ongoing discussion about the origin of WACS pattern is whether the observed temperature pattern is caused by a chain of physical processes (Honda *et al* 2009, Overland *et al* 2011, Cohen *et al* 2014, García-Serrano *et al* 2015, Jaiser *et al* 2016), or if it is part of internal variability and its occurrence results from the random sampling as revealed by the model sensitivity studies (Sun *et al* 2016, McCusker *et al* 2016, Boland *et al* 2017, Collow *et al* 2016).

We try to address this question by comparing the two Arctic warming periods (ETCAW and RAW), both characterized by decreasing BKS SIC using different reanalyses and comparing them with AGCM simulations. Using a re-analysis (ERA20C) and a model simulation (ERA20CM) using the same ECMWF atmospheric model allows us to directly infer the impact of assimilated data, since all boundary conditions are the same for both datasets.

Our results support some of the aforementioned findings concerning the RAW: Striking similarities are found between the ETCAW and RAW periods, namely the manifestation of the WACS pattern and its dynamical background, the reduced atmospheric heat transport to central Eurasia. Our study suggests that the changes in the autumn SIC in the BKS largely explain the observed temperature trends by modulating the pressure patterns in the upper troposphere, which consequently impact the heat-flux convergence over the mid-latitudes (Cohen *et al* 2014, Francis and Vavrus 2015). In this case, September sea ice concentration affects the surface turbulent heat fluxes over the BKS in the following autumn months (supplementary figure 9). Reduction in BKS sea ice can be caused by several mechanisms such as a general rise in north Atlantic SSTs (Miles *et al* 2014, Nakanowatari *et al* 2014, Årthun *et al* 2017), atmospheric heat advection (Zhang and Li 2017) or increased longwave radiation (Park *et al* 2015). Future studies are needed to address the ultimate cause behind the sea ice decrease in the ETCAW. However, we found that detrended September BKS SIC explains the zonal mean trend over Eurasia for the ETCAW better than a detrended September or DJF AMO index (supplemetary figure 10).

The main reason for the reduced heat convergence seems to be a positive geopotential height anomaly in the upper troposphere located over the BKS region, which is in agreement with recent studies concerning the RAW (Honda *et al* 2009, Petoukhov and Semenov 2010, Kim *et al* 2014, Kug *et al* 2015,

Luo *et al* 2016). Our results disagree with the findings of Sorokina *et al* (2016), who found that BKS sea ice reduction and the following turbulent heat flux over the ice-free areas is not enough to explain the WACS pattern. However, we want to underline the findings of Gastineau *et al* (2017), stating that the co-variability of sea ice, Eurasian snow and hemispheric SSTs is important for the generation of the WACS pattern. Further research is needed to address this coupled ocean–cryosphere–atmosphere pattern, which is still a challenge for recent models.

Our findings are qualitatively independent of the sea ice reconstruction at hand and it is mainly the significance of the resulting patterns that is impacted by the choice of SIC reconstruction. Interestingly, using the Walsh *et al* (2017) dataset for the ETCAW period resulted in the highest confidence for the regression analysis. Moreover, the respective ETCAW 500 hPa GPH and heat flux anomalies show a very high similarity with those obtained for the RAW period, although the sea ice reduction trend between 1911–1940 in the Walsh *et al* (2017) dataset is the weakest among the investigated SIC reconstructions.

Furthermore, our results support recent studies (Cohen 2016, Francis 2017, Gastineau *et al* 2017) which argue that current AGCMs lack the capability to properly reproduce climate feedbacks triggered by the Arctic sea ice decline. Although we found 1 out of 10 ensemble members which reproduced the WACS pattern relatively well for the analysis of trends, the regression analysis showed no connection to the underlying dynamics and disagreed with the findings from ERA20C. Additionally, the ERA20CM ensemble mean failed to reproduce the observed temperature and circulation fields for the ETCAW. Reasons for the flaws in the AGCM models can be manifold. Francis (2017) points out that boundary layer processes, troposphere–stratosphere coupling and high sensitivity to tropical climate are issues in modelling an appropriate Arctic amplification and sea ice loss response. In fact, model experiments in Tokinaga *et al* (2017) show that the correct WACS temperature pattern response is found if the model is forced mainly with tropical SST variability rather than mid-latitude SST variability. We found similar results for the ERA20CM ensemble (see supplement figure 11), underlining the points made by Cohen (2016). Smith *et al* (2017) show that modeled response to Arctic sea ice loss depends on the background state of the model and pointed out differences between AOGCMs and AGCMs response. They further noted that the response is sensitive to the detailed properties of planetary wave propagation into the stratosphere. Moreover, different factors of natural variability may play a role in the formation of the WACS pattern, which are not captured in AGCMs. Further studies are needed to investigate the disagreement between (some) GCM experiments and observed responses.

## 5. Conclusions

Several simulated and reconstructed gridded datasets were used to examine the link between September SIC in the BKS, atmospheric conditions and the WACS temperature pattern in winter. We found evidence for a manifestation of this temperature pattern not only during the current ongoing Arctic warming period (RAW), but also for the Arctic warming between 1910–1940 (ETCAW). Regression analysis with normalized SIC from the BKS region indicates that the overall temperature and heat-flux trend is largely congruent to a reduction of September BKS sea ice.

Upper troposphere conditions point towards a strengthened atmospheric blocking over the BKS, implying the advection of cold air from the polar regions to central Siberia on its eastern flank. Moreover, this blocking triggers a more meridional circulation, reducing the strength of the warm air advection by the westerlies. Comparison of the long-term climate reanalysis ERA20C with its parent model run (ERA20CM) forced by the same sea ice and SST boundary conditions suggests that this particular AGCM lacks the ability to reproduce the atmospheric conditions following low-sea ice years, both at the surface and in the upper troposphere.

These findings are consistent with several recent studies and provide the foundation for analyzing the validity of the recent theories proposing a link between reduced SIC in the BKS and the WACS. To identify the specific deficiencies in AGCMs remains an open task. Moreover, since only one AGCM was used in this study, a variety of AGCM ensemble runs are needed to clearly rule out the possibility of the occurrence of WACS pattern due to random sampling. However, future projections and impact studies of Arctic warming periods should take into account a possible deficit in the large-scale response of sea ice on the mid-latitudes in models. Upcoming high-resolution reanalyses and reconstructions will improve the understanding of the WACS during the early twentieth century and offer further insights into a possible surface–stratosphere connection triggered by sea ice reduction, snow-cover changes and decadal SST changes.

## ORCID iDs

Martin Wegmann ⓘ https://orcid.org/0000-0002-5294-2978

## References

Alekseev G, Glok N and Smirnov A 2016 On assessment of the relationship between changes of sea ice extent and climate in the Arctic *Int. J. Climatol.* **36** 3407–12

Årthun M, Eldevik T, Viste E, Drange H, Furevik T, Johnson H L and Keenlyside N S 2017 Skillful prediction of northern climate provided by the ocean *Nat. Commun.* **8** 15875

Beitsch A, Jungclaus J H and Zanchettin D 2014 Patterns of decadal-scale Arctic warming events in simulated climate *Clim. Dyn.* **43** 1773–89

Bekryaev R V, Polyakov I V and Alexeev V A 2010 Role of polar amplication in long-term surface air temperature variations and modern Arctic warming *J. Clim.* **23** 3888–906

Bengtsson L, Semenov V A and Johannessen O M 2004 The early twentieth-century warming in the Arctic—a possible mechanism *J. Clim.* **17** 4045–57

Boland E J, Bracegirdle T J and Shuckburgh E F 2017 Assessment of sea ice-atmosphere links in CMIP5 models *Clim. Dyn.* **49** 683–702

Brönnimann S, Grant A N, Compo G P, Ewen T, Griesser T, Fischer A M, Schraner M and Stickler A 2012 A multi-data set comparison of the vertical structure of temperature variability and change over the Arctic during the past 100 years *Clim. Dyn.* **39** 1577–98

Cohen J 2016 An observational analysis: tropical relative to Arctic influence on midlatitude weather in the era of Arctic amplification *Geophys. Res. Lett.* **43** 5287–94

Cohen J, Barlow M, Kushner P J and Saito K 2007 Stratosphere—troposphere coupling and links with Eurasian land surface variability *J. Clim.* **20** 5335–43

Cohen J L, Furtado J C, Barlow M, Alexeev V A and Cherry J E 2012 Asymmetric seasonal temperature trends *Geophys. Res. Lett.* **39** L04705

Cohen J, Screen J A, Furtado J C, Barlow M, Whittleston D, Coumou D, Francis J, Dethloff K, Entekhabi D and Overland J 2014 Recent Arctic amplification and extreme mid-latitude weather *Nat. Geosci.* **7** 627–37

Collow T W, Wang W, Kumar A and Zhang J 2016 How well can the observed Arctic sea ice summer retreat and winter advance be represented in the NCEP climate forecast system version 2? *Clim. Dyn.* **49** 1651–63

Connolly R, Connolly M and Soon W 2017 Re-calibration of Arctic sea ice extent datasets using Arctic surface air temperature records *Hydrol. Sci. J.* **62** 1317–40

Crasemann B, Handorf D, Jaiser R, Dethloff K, Nakamura T, Ukita J and Yamazaki K 2017 Can preferred atmospheric circulation patterns over the North-Atlantic-Eurasian region be associated with arctic sea ice loss? *Polar Sci.* **14** 9–20

De Boisséson E, Balmaseda M A and Mayer M 2017 Ocean heat content variability in an ensemble of twentieth century ocean reanalyses *Clim. Dyn.* 1–16

Dee D P and *et al* 2011 The ERA-Interim reanalysis: configuration and performance of the data assimilation system *Q. J. R. Meteorol. Soc.* **137** 553–97

Dufour A, Zolina O and Gulev S K 2016 Atmospheric moisture transport to the Arctic: assessment of reanalyses and analysis of transport components *J. Clim.* **29** 5061–81

Francis J A 2017 Why are Arctic linkages to extreme weather still up
    in the air? *Bull. Am. Meteorol. Soc.* (https://doi.org/
    10.1175/BAMS-D-17-0006.1)
Francis J A and Vavrus S J 2015 Evidence for a wavier jet stream in
    response to rapid Arctic warming *Environ. Res. Lett.* **10**
    014005
Francis J A, Chan W, Leathers D J, Miller J R and Veron D E 2009
    Winter Northern Hemisphere weather patterns remember
    summer Arctic sea ice extent *Geophys. Res. Lett.* **36** L07503
García-Serrano J, Frankignoul C, Gastineau G and De La Càmara A
    2015 On the predictability of the winter Euro-Atlantic climate:
    lagged influence of autumn Arctic sea ice *J. Clim.* **28**
    5195–216
Gastineau G, García-Serrano J and Frankignoul C 2017 The
    influence of autumnal Eurasian snow cover on climate
    and its link with Arctic sea ice cover *J. Clim.* **30**
    7599–619
Ghatak D, Deser C, Frei A, Gong G, Phillips A, Robinson D A and
    Stroeve J 2012 Simulated Siberian snow cover response to
    observed Arctic sea ice loss, 1979–2008 *J. Geophys. Res. Atmos.*
    **117** D23108
Grant A N, Brönnimann S, Ewen T, Griesser T and Stickler A 2009
    The early twentieth century warm period in the European
    Arctic *Meteorol. Z* **18** 425–32
Hansen J, Ruedy R, Sato M and Lo K 2010 Global surface
    temperature change *Rev. Geophys.* **48** RG4004
Hersbach H, Peubey C, Simmons A, Berrisford P, Poli P and Dee D
    2015 ERA-20CM: a twentieth-century atmospheric model
    ensemble *Q. J. R. Meteorol. Soc.* **141** 2350–75
Honda M, Inoue J and Yamane S 2009 Influence of low Arctic sea
    ice minima on anomalously cold Eurasian winters *Geophys.
    Res. Lett.* **36** L08707
Hori M E, Inoue J, Kikuchi T, Honda M and Tachibana Y 2011
    Recurrence of intraseasonal cold air outbreak during the
    2009/2010 winter in Japan and its ties to the atmospheric
    condition over the Barents-Kara Sea *SOLA* **7** 25–8
Inoue J, Hori M E and Takaya K 2012 The role of Barents sea ice in
    the wintertime cyclone track and emergence of a warm-Arctic
    cold-Siberian anomaly *J. Clim.* **25** 2561–8
Jaiser R, Nakamura T, Handorf D, Dethloff K, Ukita J and
    Yamazaki K 2016 Atmospheric winter response to Arctic sea
    ice changes in reanalysis data and model simulations
    *J. Geophys. Res. Atmos.* **121** 7564–77
Jaiser R, Dethloff K, Handorf D O R, Rinke A and Cohen J 2012
    Impact of sea ice cover changes on the Northern Hemisphere
    atmospheric winter circulation *Tellus A* **64** 11595
Johannessen O M, Bengtsson L, Miles M W, Kuzmina S I, Semenov
    V A, Alekseev G V, Nagurnyi A P, Zakharov V F, Bobylev L P
    and Pettersson L H 2004 Arctic climate change: observed and
    modelled temperature and sea ice variability *Tellus A* **56**
    328–41
Kaufman D S, Schneider D P, McKay N P, Ammann C M, Bradley
    R S, Briffa K R, Miller G H, Otto-Bliesner B L, Overpeck J T
    and Vinther B M 2009 Recent warming reverses long-term
    Arctic cooling *Science* **325** 1236–9
Kim B M, Son S W, Min S K, Jeong J H, Kim S J, Zhang X D, Shim
    T and Yoon J H 2014 Weakening of the stratospheric polar
    vortex by Arctic sea ice loss *Nat. Commun.* **5** 4646
King M P, Hell M and Keenlyside N 2016 Investigation of the
    atmospheric mechanisms related to the autumn sea ice and
    winter circulation link in the Northern Hemisphere *Clim.
    Dyn.* **46** 1185–95
Kretschmer M, Coumou D, Agel L, Barlow M, Tziperman E and
    Cohen J 2017 More-persistent weak stratospheric polar vortex
    states linked to cold extremes *Bull. Am. Meteorol. Soc.*
    (https://doi.org/10.1175/BAMS-D-16-0259.1)
Kug J-S, Jeong J-H, Jang Y-S, Kim B-M, Folland C K, Min S-K and
    Son S-W 2015 Two distinct influences of Arctic warming on
    cold winters over North America and East Asia *Nat. Geosci.* **8**
    759–63
Lindsay R, Wensnahan M, Schweiger A and Zhang J 2014
    Evaluation of seven different atmospheric reanalysis products
    in the Arctic *J. Clim.* **27** 2588–606

Luo D, Xiao Y, Yao Y, Dai A, Simmonds I and Franzke C L 2016
    Impact of ural blocking on winter warm Arctic–cold Eurasian
    anomalies. Part I: blocking-induced amplification *J. Clim.* **29**
    3925–47
McCusker K E, Fyfe J C and Sigmond M 2016 Twenty-five winters
    of unexpected Eurasian cooling unlikely due to Arctic sea ice
    loss *Nat. Geosci.* **9** 838–42
Miles M W, Divine D V, Furevik T, Jansen E, Moros M and Ogilvie
    A E 2014 A signal of persistent Atlantic multidecadal
    variability in Arctic sea ice *Geophy. Res. Lett.* **41** 463–9
Mori M, Watanabe M, Shiogama H, Inoue J and Kimoto M 2014
    Robust Arctic sea ice influence on the frequent Eurasian cold
    winters in past decades *Nat. Geosci.* **7** 869–73
Nakamura T, Yamazaki K, Iwamoto K, Honda M, Miyoshi Y,
    Ogawa Y and Ukita J 2015 A negative phase shift of the winter
    AO/NAO due to the recent Arctic sea ice reduction in late
    autumn *J. Geophys. Res. Atmos* **120** 3209–27
Nakamura T, Yamazaki K, Iwamoto K, Honda M, Miyoshi Y,
    Ogawa Y, Tomikawa Y and Ukita J 2016 The stratospheric
    pathway for Arctic impacts on midlatitude climate *Geophys.
    Res. Lett.* **43** 3494–501
Nakanowatari T, Sato K and Inoue J 2014 Predictability of the
    Barents sea ice in early winter: remote effects of oceanic and
    atmospheric thermal conditions from the North Atlantic
    *J. Clim.* **27** 8884–901
Opel T, Fritzsche D and Meyer H 2013 Eurasian Arctic climate over
    the past millennium as recorded in the Akademii Nauk ice
    core (Severnaya Zemlya) *Clim. Past.* **9** 2379–89
Orsolini Y J, Senan R, Benestad R E and Melsom A 2012 Autumn
    atmospheric response to the 2007 low Arctic sea ice extent in
    coupled ocean–atmosphere hindcasts *Clim. Dyn.* **38** 2437–48
Orsolini Y J, Senan R, Vitart F, Weisheimer A, Balsamo G and
    Doblas-Reyes F 2016 Influence of the Eurasian snow on the
    negative North Atlantic Oscillation in subseasonal forecasts of
    the cold winter 2009/10 *Clim. Dyn.* **47** 1325–34
Outten S, Davy R and Esau I 2013 Eurasian winter cooling:
    intercomparison of reanalyses and CMIP5 data sets *Atmos.
    Ocean. Sci. Lett.* **6** 324–31
Overland J E, Wood K R and Wang M 2011 Warm Arctic—cold
    continents: climate impacts of the newly open Arctic Sea *Polar
    Res.* **30** 15787
Overland J, Dethloff K, Francis J, Hall R, Hanna E, Kim S J, Screen J
    A, Shepherd T G and Vihma T 2016 Nonlinear response of
    mid-latitude weather to the changing Arctic *Nat. Clim.
    Change* **6** 992–9
Pages 2 K Consortium 2013 Continental-scale temperature
    variability during the past two millennia *Nat. Geosci.* **6** 339–46
Park H S, Lee S, Son S W, Feldstein S B and Kosaka Y 2015 The
    impact of poleward moisture and sensible heat flux on Arctic
    winter sea ice variability *J. Clim.* **28** 5030–40
Pedersen R A, Cvijanovic I, Langen P L and Vinther B M 2016 The
    impact of regional Arctic sea ice loss on atmospheric
    circulation and the NAO *J. Clim.* **29** 889–902
Petoukhov V and Semenov V A 2010 A link between reduced
    Barents–Kara sea ice and cold winter extremes over northern
    continents *J. Geophys. Res.* **115** D21111
Petoukhov V, Rahmstorf S, Petri S and Schellnhuber H J 2013
    Quasiresonant amplification of planetary waves and recent
    Northern Hemisphere weather extremes *Proc. Natl Acad. Sci.*
    **110** 5336–41
Poli P *et al* 2016 ERA-20C: an atmospheric reanalysis of the
    twentieth century *J. Clim.* **29** 4083–97
Ruggieri P, Kucharski F, Buizza R and Ambaum M H P 2017 The
    transient atmospheric response to a reduction of sea-ice cover
    in the Barents and Kara Seas *Q. J. R. Meteorolog. Soc.* **143**
    1632–40
Sato K, Inoue J and Watanabe M 2014 Influence of the Gulf stream
    on the Barents sea ice retreat and Eurasian coldness during
    early winter *Environ. Res. Lett.* **9** 084009
Scherhag R 1939 Die Erwärmung des Polargebiets *Annalen der
    Hydrographie* **67** 57–67
Screen J A 2017 The missing Northern European winter cooling
    response to Arctic sea ice loss *Nat. Commun.* **8** 14603

Screen J A and Simmonds I 2010 Increasing fall-winter energy loss from the Arctic Ocean and its role in Arctic temperature amplification *Geophys. Res. Lett.* **37** L16707

Semenov V A, Latif M, Dommenget D, Keenlyside N S, Strehz A, Martin T and Park W 2010 The impact of North Atlantic–Arctic multidecadal variability on Northern Hemisphere surface air temperature *J. Clim.* **23** 5668–77

Semenov V and Latif M 2012 The early twentieth century warming and winter Arctic sea ice *Cryosphere* **6** 1231–7

Serreze M C and Barry R G 2011 Processes and impacts of Arctic amplification: a research synthesis *Glob. Planet. Change* **77** 85–96

Serreze M C, Holland M M and Stroeve J 2007 Perspectives on the Arctic's shrinking sea ice cover *Science* **315** 1533–6

Shepherd T G 2016 Effects of a warming Arctic *Science* **353** 989–90

Smith D M, Dunstone N J, Scaife A A, Fiedler E K, Copsey D and Hardiman S C 2017 Atmospheric response to Arctic and Antarctic sea ice: the importance of ocean-atmosphere coupling and the background state *J. Clim.* **30** 4547–65

Sorokina S A, Li C, Wettstein J J and Kvamstø N G 2016 Observed atmospheric coupling between Barents Sea ice and the warm-Arctic cold-Siberian anomaly pattern *J. Clim.* **29** 495–511

Stroeve J C, Maslanik J, Serreze M C, Rigor I, Meier W and Fowler C 2011 Sea ice response to an extreme negative phase of the Arctic Oscillation during winter 2009/2010 *Geophys. Res. Lett.* **38** L02502

Sun L, Perlwitz J and Hoerling M 2016 What caused the recent Warm Arctic, cold continents trend pattern in winter temperatures? *Geophys. Res. Lett.* **43** 5345–52

Suo L, Gao Y, Guo D, Liu J, Wang H and Johannessen O M 2016 Atmospheric response to the autumn sea ice free Arctic and its detectability *Clim. Dyn.* **46** 2051–66

Titchner H A and Rayner N A 2014 The Met Office Hadley Centre sea ice and sea surface temperature data set, version 2: 1. Sea ice concentrations *J. Geophys. Res. Atmos.* **119** 2864–89

Tokinaga H, Xie S P and Mukougawa H 2017 Early 20th-century Arctic warming intensified by Pacific and Atlantic multidecadal variability *Proc. Natl Acad. Sci.* **114** 6227–32

Vihma T 2014 Effects of Arctic Sea ice decline on weather and climate: a review *Surv. Geophys.* **35** 1175–214

Walsh J E, Fetterer F, Scott Stewart J and Chapman W L 2017 A database for depicting Arctic sea ice variations back to 1850 *Geogr. Rev.* **107** 89–107

Wegmann M, Orsolini Y, Vázquez M, Gimeno L, Nieto R, Bulygina O, Jaiser R, Handorf D, Rinke A and Dethloff K 2015 Arctic moisture source for Eurasian snow cover variations in autumn *Environ. Res. Lett.* **10** 054015

Wegmann M, Brönnimann S and Compo G P 2017 Tropospheric circulation during the early twentieth century Arctic warming *Clim. Dyn.* **48** 2405–18

Wood K R and Overland J E 2010 Early 20th century Arctic warming in retrospect *Int. J. Climatol.* **30** 1269–79

Wu B 2017 Winter atmospheric circulation anomaly associated with recent Arctic winter warm anomalies *J. Clim.* **30** 8469–79

Zhang J, Tian W, Chipperfield M P, Xie F and Huang J 2016 Persistent shift of the Arctic polar vortex towards the Eurasian continent in recent decades *Nat. Clim. Change* **6** 1094–9

Zhang L and Li T 2017 Physical processes responsible for the interannual variability of sea ice concentration in Arctic in boreal autumn since 1979 *J. Meteorol. Res.* **31** 468–75